VERSITA

Cent. Eur. J. Chem. • 7(2) • 2009 • 168–174
DOI: 10.2478/s11532-009-0018-y

Central European Journal of **Chemistry**

# Bioresorbable carbonated hydroxyapatite $Ca_{10-x}Na_x(PO_4)_{6-x}(CO_3)_x(OH)_2$ powders for bioactive materials preparation

**SSC-2008**

Elena S. Kovaleva[1*], Maxim P. Shabanov[1], Valery I. Putlyaev[1], Yury D. Tretyakov[1], Vladimir K. Ivanov[2], Nikolay I. Silkin[3]

[1] *Department of Materials Science Lomonosov Moscow State University, 119992, Moscow, Russia*

[2] *Laboratory of Chemical Synergy Kurnakov Institute of General and Inorganic Chemistry of RAS, 119991, Moscow, Russia*

[3] *Department of Radio Spectroscopy and Quantum Electronics Kazan State University, 420008, Kazan, Russia*

**Received 04 July 2008; Accepted 01 November 2008**

**Abstract:** The purpose of this work was to find and investigate a correlation between the carbonate ion content in crystalline lattice and defect structure, and solubility of the materials; finally, to prepare the materials under study for *in vitro* tests. Various techniques, such as XRD, FTIR, TEM, FESEM/EDX, TG/DTA, AES (ICP), wet chemical analysis, Ca-ionometry, microvolumetric analysis of evolved $CO_2$, BET adsorption, were applied to determine the efficiency of carbonate substitution, and to quantify the elemental composition, as well as to characterize the structure of the carbonated hydroxyapatite and the site(s) of carbonate substitution,. It was shown that AB-type substitution prevails over other types with the carbonate content increase. According to *in vitro* tests, the bioactivity of the samples is correlated with the carbonate content in carbonate-doped hydroxyapatite due to accumulation of defects in carbonated hydroxyapatite nanocrystals.

**Keywords:** *Carbonated hydroxyapatite • Aliovalent doping • Microstructure • Resorption.*



## 1. Introduction

There is a strong need to replace bone substance lost due to both traumatic and non-traumatic events. Synthetic hydroxyapatite $Ca_{10}(PO_4)_6(OH)_2$(HA) has been widely used as a material for biomedical applications due to its chemical composition mirroring that of bone mineral [1,2]. However, human bone mineral differs in composition from stoichometric HA in that it contains additional ions, of which carbonate is the most abundant specie (ca. 8 wt.%) [3,4].

It is known that chemical modification of HA results in an increase in the dissolution rate and osteoinductive properties of implants [2]. In particular, the incorporation of carbonate ions has a considerable influence on the physicochemical properties of the solid and, hence, on the mineralization, demineralization, and remineralization processes [1,3]. Introduction of carbonate ions in the HA would increase its dissolution rate in solution and could enhance its osteointegration rate [1,5]. Thus, carbonated hydroxyapatite is a prospective material for bone healing in order to mimic the composition of native bone since it is both more soluble and bioactive than stoichiometric HA [1,2,5].

Carbonate ion can substitute at two sites in the apatite structure, either, the hydroxyl or the phosphate

* *E-mail: alenakovaleva84@mail.ru*

ion positions, giving A- and B-type carbonated hydroxyapatite (CHA), respectively [3,4,6]. In addition, sodium ions, found in bone, are also known to increase the maximum ratio of carbonate substitution in B- site, because its incorporation in calcium sites induces a favorable electrical charge balance [6]. The role of carbonate on the biological behavior of pure single phased carbonated hydroxyapatites without alkali remains unclear. Therefore, it is of fundamental importance to know the mechanism for carbonate incorporation in hydroxyapatite. AB-type carbonated hydroxyapatite with varying and controlled amounts of carbonate ions in A and B sites of the apatite structure has never been carefully evaluated for the effect of carbonate content on microstructure and resorption *in vitro* [1,6,7].

# 2. Experimental Procedures

## 2.1. Materials preparation

Carbonated hydroxyapatite nanopowders with various degrees of carbonate substitution were prepared by an aqueous precipitation method according to the following equation:

$$(10-x)Ca(NO_3)_2+(6-x)(NH_4)_2HPO_4+xNa_2CO_3+(8-x)NH_4OH \rightarrow Ca_{10-x}Na_x(PO_4)_{6-x}(CO_3)_x(OH)_2+(20-3x)NH_4NO_3+xNaNO_3+(6-x)H_2O,$$

where x = 0, 0.25, 0.5, 0.75, 1, 1.5, 2, by drop-wise addition of 0.3 M stock solution of ammonium phosphate ($(NH_4)_2HPO_4$, 99.9%, Labteh, Russia) with appropriate amount of sodium hydrogencarbonate ($NaHCO_3$, 99.9%, Labteh, Russia) to 0.5 M stock solution of calcium nitrate ($Ca(NO_3)_2 \cdot 4H_2O$, 99.9%, Labteh, Russia). Prior to making the stock solutions all of the reagents were checked for the content of main substances by gravimetric or titrimetric chemical analyses. The pH value of the stock solutions was pre-adjusted to 11.5 by addition of $NH_4OH$ (30 wt.%), and then maintained manually at the constant value of 12.0 (± 0.5) by addition of concentrated ammonium hydroxide. An Expert-001 pH-meter (Econix, Russia) with an ESK-1030 glass electrode (Russia) was used to monitor pH. Temperature was controlled and regulated at 80 ± 1°C. After total mixing of the stock solutions, the suspension was ripened and heated by use of a thermostatically controlled hot plate for 24 hours under constant stirring. Then, a precipitate was filtered and washed with 300 mL of distilled water. The resulting precipitate was dried at room temperature in air. Dry powders were heat treated for 1 hour at 260°C in air in order to reach better crystallinity and to eliminate adsorbed moisture and other synthesis residues such as nitrous species. It was concluded that this thermal treatment did not affect the structure of the precipitates since the lattice parameters change minimally (less then 0.005 Å), there were no differences in IR spectra, and the Ca/P ratio remained unchanged.

## 2.2. Materials characterization

The as-received and heat treated powders were studied by X-ray diffraction analysis in the interval of angles 2Θ = 10 - 110° (Cu Kα radiation, Rigaku D/MAX 2500 with rotating anode) and IR spectroscopy in 400-4000 $cm^{-1}$ range (pellets: 1 mg of powder in 150 mg of analytical grade KBr, Ø = 13 mm, Perkin-Elmer 1600 FTIR spectrophotometer, USA). Sizes of crystallites and microstrain parameters were extracted from X-ray diffraction line profile using Scherrer- and Wilson-formulas from Williamson-Hall-plots according to the procedure of de Keijser, Langford, Mittemeijer *et al*. [8] with the help of STOE WinXPOW software (STOE&Cie GmbH, Germany).

The micromorphology of the powders was examined by scanning and transmission electron microscopy (JEM-2000FX II, JEOL, Japan, operated at 200 kV; and FESEM LEO SUPRA 50VP, Carl Zeiss, Germany, 5 kV).

The Ca-content of the CHA precipitates was quantified by EDTA titration. Phosphorous content was determined using the quinolinium phosphomolybdate method modified by Dahlgren [9]. The content of Na was determined using AES (ICP) with Optima 5300DV (Perkin-Elmer, USA). In some cases the Ca/P ratio of the CHA samples was obtained independently from EDX data (INCA Energy+, Oxford Instruments, UK, attached to LEO SUPRA 50 VP). The carbonate content was analyzed with microvolumetric determination of $CO_2$ released from the samples after their dissolution in nitric acid. The overall content of $CO_2$ and $H_2O$ was examined by TG/DTA (Diamond Pyris, Perkin Elmer, USA, quasi-isothermal heating to maintain a decomposition rate at 10 μg $min^{-1}$; STA 409 PC, Netzsch, Germany, with IR-analysis of evolved gases). The specific surface area of each carbonated hydroxyapatite was determined by BET method with nitrogen as adsorbate (Nova 4200e, Quantachrome, USA).

Bioactivity of the CHA samples was assessed *in vitro* using experiments on dissolution (resorption) of the samples in acidic media and precipitation of an apatite layer on the surface of the samples from supersaturated solutions under physiological pH. Dissolution rates of CHA samples were studied by measuring pCa (pH-meter-ionomer Expert-001, Econix, Russia,

computer acquiring a signal with a time interval of 1 s) of 0.1 g of the sample in 100 mL of 0.1 M acetate buffer (pH = 5.5) at 37°C for up to 24 hours. The specific dissolution rate, w ($m^2\ g^{-1}\ s$), was calculated as

$$w = \frac{d(\mathrm{pCa})/dt\big|_{t=0}}{(\mathrm{pCa}_0 - \mathrm{pCa}_\infty)\cdot s}$$

from experimental curves pCa = *f(t)*, where $pCa_0$ is the initial value of pCa (at *t = 0*), and $pCa_\infty$ is the asymptotic value at the end of experiment, s is specific surface of the sample ($m^2\ g^{-1}$). In precipitation experiments, simulated body fluid (SBF) media was used (142 mM $Na^+$, 5 mM $K^+$, 1.5 mM $Mg^{2+}$, 2.5 mM $Ca^{2+}$, 147.8 mM $Cl^-$, 27 mM $HCO_3^-$, 1 mM $HPO_4^{2-}$, $SO_4^{2-}$, Tris-buffer, pH = 7.4 ). SBF was prepared in accordance with a chemical composition of human body fluid, with ion concentrations nearly equal to those of the inorganic constituents of human blood plasma, following Kokubo *et al*. [10]. Pelletized samples were soaked in SBF for different time intervals (from 7 to 21 days) at 37°C and pH 7.4. Afterward, they were examined with SEM to analyze a fresh apatite layer precipitated from SBF.

## 3. Results and Discussion

X-ray diffraction (XRD) analysis showed the diffraction patterns that correspond to those of CHA (# 9-432 from ICDD PDF-2) for all samples (Fig. 1). The as-received powders were found to be nanocrystalline as it was evidenced from broad diffraction peaks, and free of secondary phases. Thus, an increase in the carbonate content is associated with a decrease in crystallite sizes in agreement with Gibson *et al.* [3]. Carbonate substitutions in hydroxyapatites are known to change the crystal lattice parameters. It is widely accepted that a pure type A causes extension of the *a*- and contraction of the *c*-axis parameters, in contrast, a pure type B carbonated apatite causes contraction of the *a*- and expansion of the *c*-axis dimensions. Unfortunately, published data concerning this issue are still controversial, *e.g.* Barralet *et al.* [11] reported on maximum in a *vs* carbonate content dependence and opposite behavior for *c*-axis (though the last dependence was only claimed but not presented in the article) , while Pieters *et al.* [12] did not find any correlation between carbonate content and the lattice parameters. According to this work, the effect of carbonate content on lattice parameters and cell volumes of the powders under

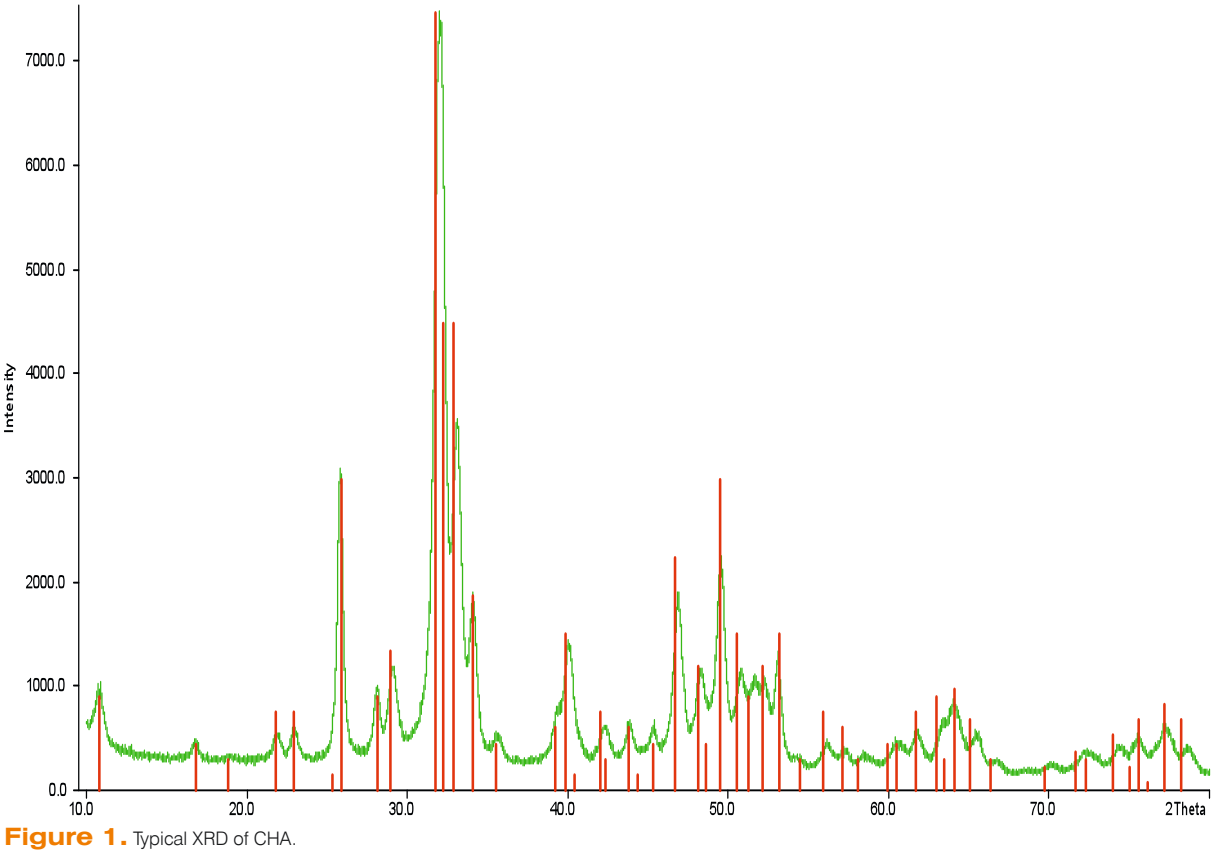


**Figure 1.** Typical XRD of CHA.

study evaluated with XRD is rather complex (Fig. 2 and Table 1). However, coupling XRD, FTIR, and TG/DTA data, one can isolate the following regions along the *x*-axis and ascribe certain substitution types:

**Table 1.** Lattice parameters and cell volumes of CHA powders ($P6_3/m$), after heat treatment 260°C per 1 hour

| x from $Ca_{10-x}Na_x(PO_4)_{6-x}(CO_3)_x(OH)_2$ | a, Å | c, Å | V, Å³ |
|---|---|---|---|
| x = 0 | 9.402(2) | 6.890(1) | 527.5(2) |
| x = 0.25 | 9.408(2) | 6.898(3) | 528.7(3) |
| x = 0.5 | 9.376(2) | 6.893(2) | 524.8(2) |
| x = 0.75 | 9.355(3) | 6.890(2) | 522.2(3) |
| x = 1 | 9.356(3) | 6.889(2) | 522.3(3) |
| x = 1.5 | 9.335(4) | 6.894(3) | 520.3(5) |
| x = 2 | 9.337(3) | 6.904(2) | 521.3(2) |

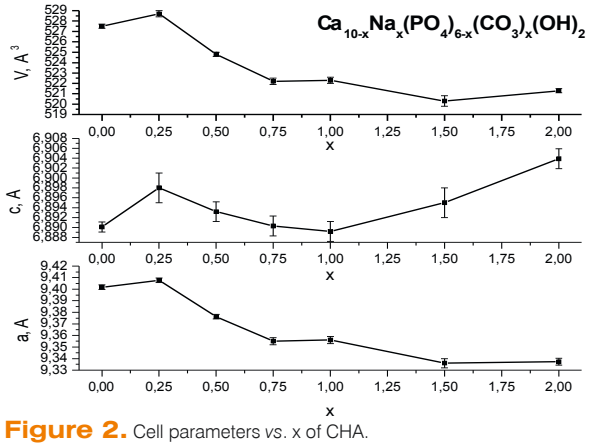


**Figure 2.** Cell parameters *vs.* x of CHA.

i) $x$ = 0 - 0.25, with slight expansion of lattice volume related, presumably, to A-type,
ii) $x$ = 0.25 - 0.75, transition region revealing noticeable volume contraction of the lattice ($\Delta V/V$ = -1.2%); importantly, only for the samples with $x$ = 0.25 and 0.5, non-zero values of microstrain, compensated within the bulk of a crystallite, were extracted from the XRD profile analysis (ε = 0.1% for both samples, assuming a Young modulus for apatite $E$ = 100 GPa, corresponding to a density of elastic energy $U_{elast} = 0.5E\varepsilon^2$ = 50 kJ m$^{-3}$); the origin of these contractive microstrains lies in different sizes of $CO_3^{2-}$ and $PO_4^{3-}$ (*i.e.* the reason underlying such a behavior of the lattice in this region is a B-type substitution ),
iii) $x$ > 0.75, slight contraction of lattice volume with increasing $x$, however, without detectable microstrain, that implies further filling of B-positions with an effective compensation mechanism (relaxation) of substitution microstrains; a possible relaxation channel could be redistribution of $CO_3^{2-}$ between B- and A-sites, thus, this region corresponds to CHA of AB-type.

Transmission electron microscopy (TEM) observations showed the powders with HA crystals less than 100 nm, agglomerated into bigger particles. Switching of particle shape from a needle-like to a spherical one is observed as the carbonate content increases. It is of note that in some cases (for intermediate values of $x$) it was possible to observe two different types of morphology within the same sample. We believe that this fact is an indication of a non-uniform distribution of carbonate ions over the samples, coming from variation of the composition across a reaction vessel. Another TEM-observation, inconsistent with available literature, was that well-resolved mesoporosity

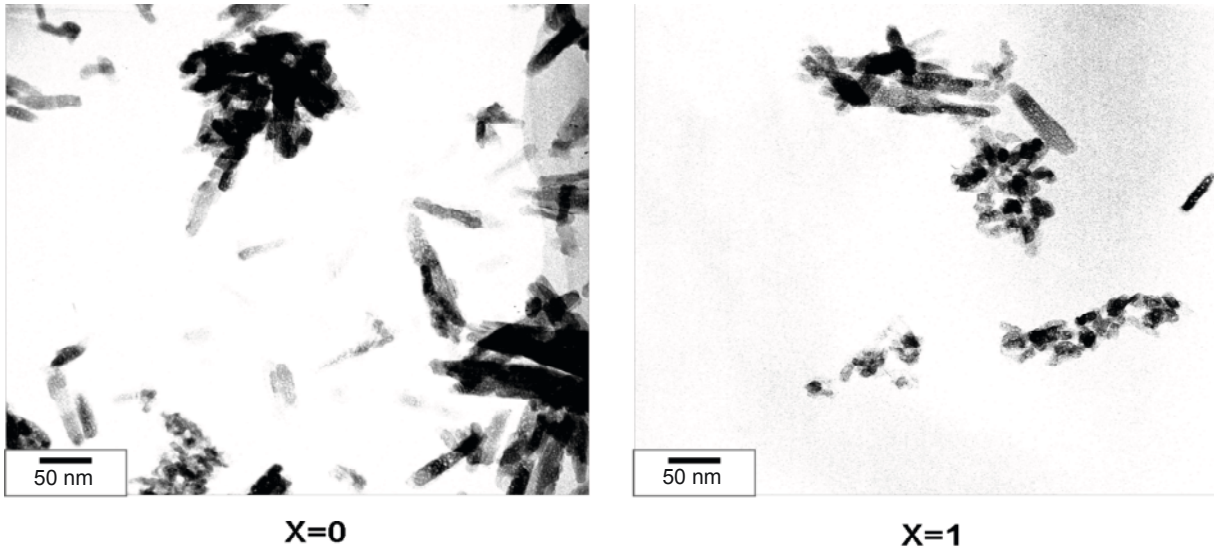


**Figure 3.** TEM image of CHA powders (x = 0, 1)

of the samples varied non-monotonously with *x* (Fig. 3). The pores filled with a mother solution can be decrypted at 500 - 800°C according to TG/DTA. Let us underline here that the sizes of crystallites deduced from XRD profile analysis were systematically lower than the dimensions determined by TEM. Another feature consisted in that XRD crystallite sizes (for both [001] and [100] directions) had a tendency to decreased with increase of x, however, non-monotonously, with a maximum around x = 0.5 - 0.75). The opposite behavior demonstrated variation of specific surface values with x. Bearing in mind distinct mesoporosity of the samples, it becomes clear that the crystallite sizes obtained from XRD line broadening (or the volume of coherent scattering) refer more to interpore distance than to overall dimensions of a mesoporous body. Apparently, this distance is maximal for the samples from the transition region with *x* = 0.25 - 0.75, and, hence, the porosity of these samples is minimal. Being the most bulky, these samples concentrate substitution stresses to a greater extent compared to other porous samples; this conclusion is consistent with the observation of the trend in the lattice parameters. The (mean over the sample) values of the lattice parameters reflect a distribution of the dopant across the crystals, the sizes of crystals and their porosity, which undoubtedly depend on conditions of synthesis (temperature, pH, ripening time).Thus, the discrepancy in the trends of CHA lattice parameters presented by different authors with an increase of carbonate content becomes clear.

The FTIR spectra (Fig. 4) showed that all the compositions exhibited the characteristic bands of phosphate groups of the apatite structure at about 550 and 600 $cm^{-1}$ ($v_4$), 960 $cm^{-1}$ ($v_1$), 1020 - 1120 $cm^{-1}$ ($v_3$). There are two regions in the spectra which characterize carbonate vibrations: 850 - 890 $cm^{-1}$ ($v_2$ vibrations of carbonate groups), 1400 - 1650 $cm^{-1}$ ($v_3$ vibrations of carbonate groups in apatites). The region of $v_2$-type vibrations of carbonate groups is expanded in Fig. 4. The bands were assigned to carbonate vibrations in A- or B-site of the apatite lattice in accordance with the literature data [1]. Summing up, the carbonate ions are likely to be located in B-sites. However, from detailed examination of these IR spectra the presence of carbonate in A-sites can not be totally excluded. Thus, all the powders should be considered as AB-type carbonated apatites. The bands at 630 and 3540 $cm^{-1}$ were assigned to OH-groups of the apatite structure. The relative intensity of these bands decreased as the carbonate content increased. The broad bands in the regions 1600 - 1700 and 3200 - 3600 $cm^{-1}$ correspond to adsorbed water. The band at 1380 $cm^{-1}$ was attributed to residual nitrates, resulting from synthesis precursors. It was particularly visible in the IR spectrum of HA powder that was not washed after synthesis (HA, *x* = 1). By and large, the regularities of carbonate substitution deduced from FTIR-spectra agree fairy well with those found with XRD and discussed above.

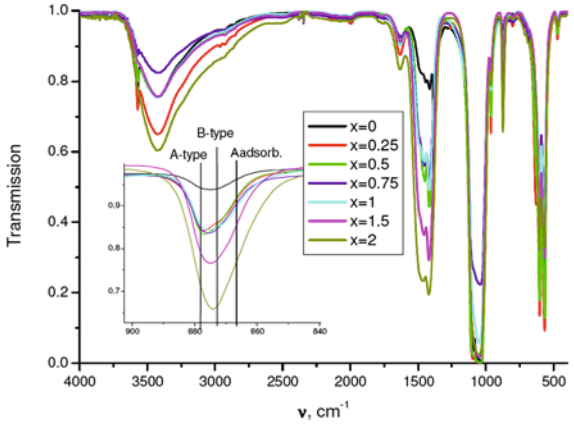


**Figure 4.** FTIR-spectra of CHA.

The atomic ratios of Ca/P, Na/Ca, $CO_3^{2-}/PO_4^{3-}$ of CHA

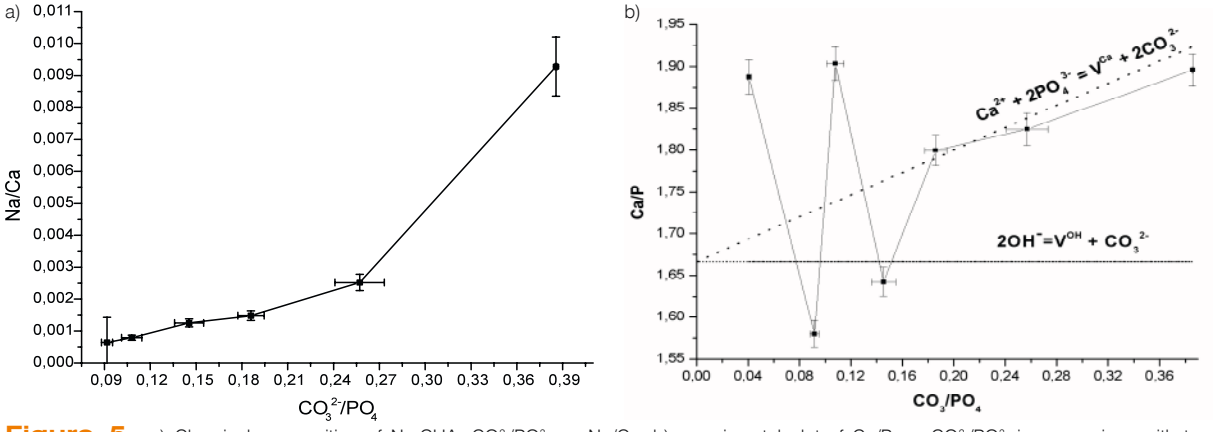


**Figure 5.** a) Chemical composition of Na-CHA: $CO_3^{2-}/PO_4^{3-}$ *vs.* Na/Ca, b) experimental plot of Ca/P *vs.* $CO_3^{2-}/PO_4^{3-}$ in comparison with two substitution models.

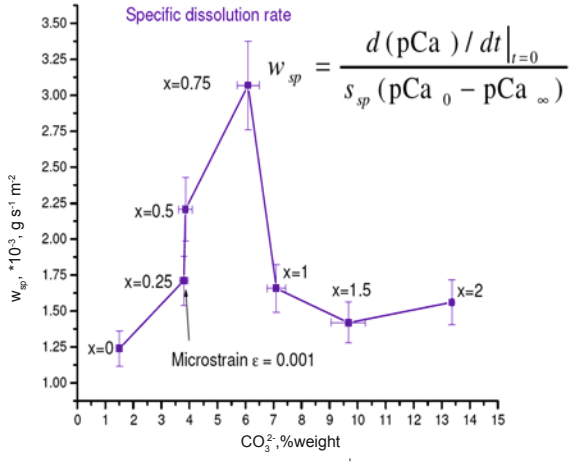


**Figure 6.** Dissolution rate of CHA in acetate buffer solution.

samples were calculated from the results of chemical analysis. Fig. 5a shows insignificant incorporation of Na into the crystal lattice. In order to obtain more information on the substitution mechanism (*viz.* charge compensation in the course of aliovalent doping), experimental plots of Ca/P *vs* $CO_3^{2-}/PO_4^{3-}$ were compared with two models (Fig. 5b):

1) model B related to the quasi-chemical equation $Ca^{2+} + 2PO_4^{3-} = V_{Ca} + 2CO_3^{2-}$, and to the formula $Ca_{(10-x/2)}(PO_4)_{(6-x)}(CO_3)_x(OH)_2$;

2) model A related to the quasi-chemical equation $2OH^- = V_{OH} + CO_3^{2-}$, and to the formula $Ca_{10}(PO_4)_6(OH)_{2-2x}(CO_3)_x$.

The slope of the experimental plot matches well model B in the region $x > 0.75$. Thus, chemical analysis confirms the substitution scenario made on the basis of structural techniques (see above). The molecular formula of the samples were derived from both structural and analytical data. Two points are essential for deriving the formula: (i) independent filling of A- and B-positions accompanied by formation of vacancies in $OH^-$ and Ca-sites, respectively, and (ii) redistribution of the dopant between A- and B-sites evoking relaxation of the lattice from substitution stresses. Thus, CHA AB-type (assuming insignificant incorporation of Na) could be presented as:
$(Ca_{10-xu/2}V_{xu/2})\{(PO_4)_{6-xu}(CO_3)_{xu}\}[(OH)_{2(1+yu-y)}(CO_3)_{y(1-u)}V_{y(1-u)}]$,
where ( ) – positions of Ca, { } stands for positions of B-type, [ ] – for positions of A-type, V denotes a vacancy, parameter $0 < x < 6$ reflects occupancy of B-type positions, and parameter $0 < y < 1$ does the same for A-type, parameter $0 < u < 1$ describes a transition between B- and A-positions similar to the well-known parameter of inversion for spinel structure.

Bioactivity of each sample was evaluated *in vitro* using two kinds of experiments: 1) dissolution in acetate media simulating active resorption with osteoclastic cells, and 2) dissolution-precipitation phenomena in SBF solutions at near physiological pH values representing the activity of the material with respect to blood plasma.

A correlation between dissolution rate of CHA in acetate buffer and microstrain/size of crystals was revealed (Fig. 6). It is worth noting that the specific dissolution rate (normalized to unit surface) demonstrated quite a sharp gain around the point of the substitution mechanism changing (x = 0.25 - 0.75); this area also featured pronounced microstrains (*ca.* 0.1%) found in CHA nanocrystals as it was observed by XRD profile analysis. It was shown above that these microstrains correspond to $U_{elast} \approx 50$ kJ m$^{-3}$ (or, assuming density of CHA ≈ 3 g cm$^{-3}$ [13], to ≈ 0.02 kJ mol$^{-1}$). This contribution to the overall energy balance of a crystal looks quite subtle, however, it has a significant influence on the

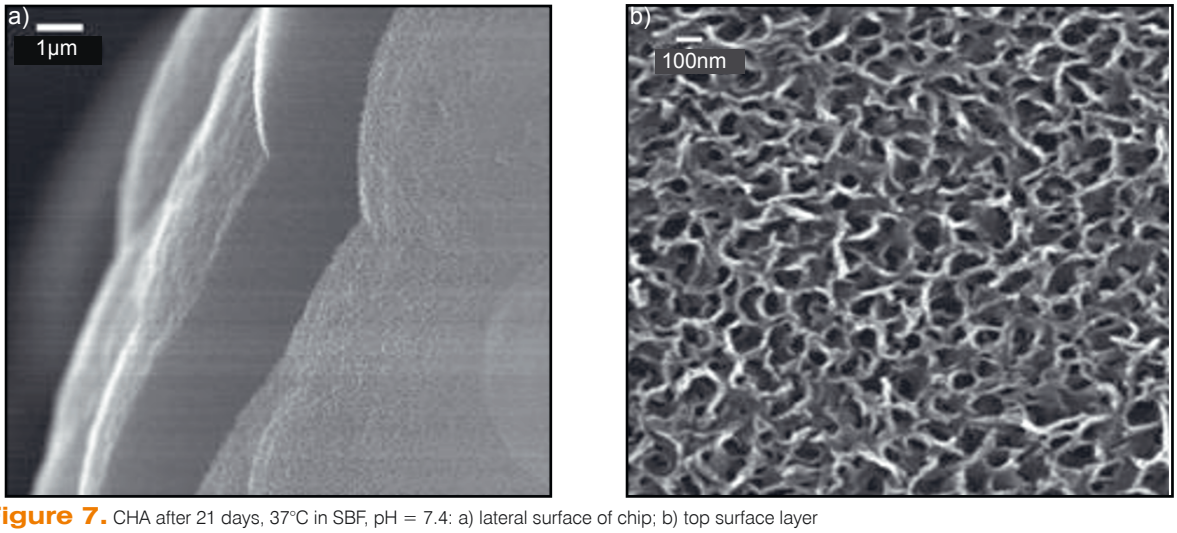


**Figure 7.** CHA after 21 days, 37°C in SBF, pH = 7.4: a) lateral surface of chip; b) top surface layer

dissolution rate. Then, we have to conclude that this elastic energy is accumulated in a volume less than the volume of a crystallite (and this is consistent with the nature of microstrains causing X-ray line broadening; corresponding stresses are to be balanced within the volume of a crystallite), and it is attributed to a non-uniform distribution of the dopant across the crystal coming from non-equilibrium conditions of synthesis. This subject was extensively discussed with respect to the composition of a distorted surface layer in biogenic apatite nanocrystals (see, *e.g.* [14]). As to overall dissolution rate (not normalized to unit surface), it grows with the increase of the carbonate content.

The dissolution-precipitation of CHA under physiological pH was evaluated *in vitro* using SBF media. Samples were soaked in SBF for different time intervals (from 7 to 21 days) at 37°C and pH 7.4. Afterward, they were examined with SEM to detect a fresh apatite layer precipitated from SBF. It is quite clear from Fig. 7a, that formation of the apatite layer on the surface of the materials is observed. After 7 days of immersion in SBF the surface of bioactive material was covered by an open-work layer consisting of plate-like self-organized particles of newly formed carbonate apatite (Fig. 7b). This layer becomes thicker as the carbonate content in CHA increases.

Finally, growth of carbonate content in CHA gives rise to defects of the crystal lattice and specific patterns of microstructure; of these, there are vacancies in Ca- and OH-sublattice, non-uniform distributions of the dopant across the crystal volume, and distinct mesoporosity of the crystals. Accumulation of these defects leads to higher solubility of CHA crystals and, thus, to better bioactivity.

## 4. Conclusions

The chemical composition of AB-type CHA nanopowders could be described with the following formula: $(Ca_{10-xu/2}V_{xu/2})\{(PO_4)_{6-xu}(CO_3)_{xu}\}[(OH)_{2(1+yu-y)}(CO_3)_{y(1-u)}V_{y(1-u)}]$, where ( ) stands for positions of Ca, { } – for positions of B-type, [ ] – for positions of A-type, and V denotes a vacancy.

It was shown that there is insignificant incorporation of Na into the crystal structure of HA. Over the range of 0 - 4% wt. ($x < 0.25$), the substitution of $OH^-$ by $CO_3^{2-}$ takes place leading to A-Type of CHA, further increase of $CO_3^{2-}$-content enhances $PO_4^{3-}$-substitution giving AB-type of CHA.

Higher dissolution rates of CHA powders (in comparison with pure HA) were observed during the experiments in buffered solutions at pH = 5.5 and in SBF. The increase of the dissolution rate can be related to intrinsic microstrains in the HA crystals due to the significant difference in effective ionic radii of carbonate and phosphate groups.

According to *in vitro* tests, the bioactivity of the samples increases with the growth of carbonate content in carbonate-doped HA due to accumulation of defects in the CHA nanocrystals.

## Acknowledgements

The work was partially supported by RFBR grants 05-03-32768, 07-08-50256, 09-03-01078 and Federal Program „R&D in priority directions of science and technology in Russia for the period of 2007-2012 years" (state contracts №№ 02.513.11.3159, 02.513.11.3160).

The authors gratefully acknowledge the contribution of Dr I.V. Fadeeva and Dr V.S. Komlev for help in material preparation.

## References

[1] J.P. Lafon, E. Champion, D. Bernache-Assollant, J. Eur. Cer. Soc. 28, 139 (2008)
[2] R.Z. LeGeros, Clin. Orthoped. Rel. Res. 395, 81 (2002)
[3] I.R. Gibson, W. Bonfield, J. Biomed. Mater. Res. 59, 697 (2002)
[4] L.G. Ellies, D.G.A. Nelson, J.D.B. Featherstone, J. Biomed. Mater. Res. 22, 541 (1988)
[5] A. Ito, K. Maekawa, S. Tsutsumi, F. Ikazaki, T. Tateishi, J. Biomed. Mater. Res. 36, 522 (1997)
[6] M. Vignoles, G. Bonel, D.W. Holcomb, R.A. Young, Calcif. Tissue Int. 43, 33 (1988)
[7] F.C.M. Driessenrs, PhD thesis, Edinburgh University (Edinburgh, UK, 1995)
[8] T. De Keijser, J.I. Langford, E.J. Mittemeijer, A.B.P. Vogels, J. of Appl. Cryst. 15, 3087 (1982)
[9] S.E. Dahlgren. Z. Analyt. Chem. 189, 243 (1962)
[10] T. Kokubo, H. Kushitani, S. Sakka, T. Kitsugi, Y. Yamamuro. J. Biomed. Mater. Res. 24, 721 (1990)
[11] J. Barralet, S. Best, W. Bonfild. J. Biomed. Mater. Res. 41, 79 (1998)
[12] I.Y. Pieters, E.A.P. De Maeyer, R.M.H. Verbeeck, Inorg. Chem. 35, 5791 (1996)
[13] T. Kanazawa, Inorganic phosphate materials (Elsevier Science Publishing, Amsterdam, 1989)
[14] J.D. Pasteris, B. Wopenka, J.J. Freeman, K. Rogers, E. Valsami-Jones, J.A.M. van der Houwen, M.J. Silva. Biomat. 25, 229 (2004)